Analysis of Heating Effects and Deformations for a STAF Panel with a Coupled CFD and FEM Simulation Method

Daniel Brandl[1*], Helmut Schober[2], Christoph Hochenauer[1]

* Corresponding author
1 Graz University of Technology/ Institute of Thermal Engineering, Austria, daniel.brandl@tugraz.at
2 Graz University of Technology/ Institute of Building Construction, Austria

Abstract

Conventional sandwich panels are one of the cheapest and easiest solutions for forming the thermal building envelope of industrial buildings. They are pre-fabricated façade elements, of which millions of square metres have been produced and mounted every year. There is great potential to reduce the consumption of fossil fuels and CO2 emissions through the solar thermal activation of such a sandwich panel. In the course of the research project ABS-Network SIAT 125, a Solar Thermal Activated Façade (STAF) panel was designed which is to be optimised both thermally and structurally. This study shows a first version of a so-called 'one way coupled' thermal and structural analysis of a conventional sandwich panel compared to the STAF panel. For this purpose, the numerical methods of Computational Fluid Dynamics (CFD) and Finite Element Method (FEM) are used together in one simulation environment. Furthermore, results from an outdoor test facility are presented where a first version of a STAF panel is tested under real climate conditions. The CFD model was positively evaluated by comparing measured and computed temperatures.

Keywords

Solar Thermal Activated Façade (STAF) Panel, Computational Fluid Dynamics (CFD), Finite Element Method (FEM), outdoor measurements

DOI 10.7480/jfde.2018.3.2567

1 INTRODUCTION OF THE STAF PANEL

1.1 DEVELOPMENT APPROACH

Conventional sandwich panels are some of the cheapest and easiest solutions for forming the thermal building envelope of industrial buildings (BKI 2018). They are pre-fabricated façade elements, of which millions of square metres have been produced and mounted every year (Koschade, 2011; IC Market Tracking, 2016). Sandwich panels consist of both an interior as and exterior metal plate (steel and aluminium are widely used) with thermal insulation (for example expanded polystyrene "EPS" or mineral wool "MW") in between (EN 14509).

The basic idea of the Interreg project "ABS-Network SIAT 125" is the solar thermal activation of a conventional sandwich panel. In this case, thermal activation means the conversion of solar energy to provide energy for the production of domestic hot water and/or heating and cooling applications. Thanks to a functionally convincing and creatively sophisticated revision of sandwich panels, the field of application can be extended to office buildings, residential buildings, buildings for education, etc. In the field of research, studies were more focused on the variation of different compositions as thermal insulation, in order to improve both the static and the thermal behaviours. Authors presented studies using foam core as thermal insulation (Missoum, Lacaze, Amabili, & Alijani, 2017; Qintana & Mower, 2017), honeycomb structure (Ebrahimi, Someh, Norato, & Vaziri, 2018) and different filling materials like aluminium (Li, Zheng, Yu, & Lu, 2017), blockboard and batternboard (Haseli, Layeghi, & Hosseinabadi, 2018), ceramic, silicon, or carbon (Yuan et al., 2018), cellulose (Yazdani Sarvestani, Akbarzadeh, Niknam, & Hermenean, 2018) or even concrete (Hashemi, Razzaghi, Moghadam, & Lourenço, 2018). The approach of using a solar thermally activated sandwich panel has not yet been found in the actual state of the science.

1.2 PRODUCTION CONCEPT AND WORKING PRINCIPLE OF THE STAF-PANEL

The metal sheets of the so-called 'Solar Thermal Activated Façade' (STAF) panel have integrated fluid pipes that can be produced by the so-called 'Roll-Bonding' fabrication method (Eizadjou, Manesh, & Janghorban, 2009). With this special metal-forming technique, two sheets are combined to one steel plate whereby the fluid pipes are produced by inflation (one-sided or double-sided inflation). In the case of the one-sided inflation method, only one metal sheet is deformed, whereas an equilateral deformation is realised in the double-sided inflation method. The exterior plate acts as an absorber of a solar thermal collector for the conversion of solar energy into hot water, whereas the interior plate can be used for heating and cooling of the interior rooms. The company Talum d.d. (Talum, 1942) is using this technology in order to produce absorber plates for evaporators of refrigerators. Fig. 1 shows a photo of a STAF panel which is equipped with double side inflated aluminium absorbers.

The absorbers were produced by Talum d.d. in Kidricevo Slovenia, and the sandwich panel was finalised at the company Brucha Ges.m.b.H. in Michelhausen Austria (Brucha, 1948), where the thermal insulation was filled between the interior and exterior absorber plate. This STAF panel, with dimensions of 1.75 x 0.5 x 0.15m, was used in the outdoor measurements presented in Chapter 2. The actual state of the science reveals a number of studies in which two main applications for roll-bonded plates were found. One application is the use of roll-bond heat exchangers used as evaporators in cooling systems and refrigerators (Ravi, Krishnaiah, Akella, & Azizuddin, 2015;

Hermes, Melo, & Negrão, 2008; Righetti, Zilio, & Longo, 2014), while the other application is the use of a roll-bonded thermal absorber for conversion of solar energy and hot water production (Sun ,Wu, Dai, & Wang, 2014; Del Col, Padovan, Bortolato, Dai Prè, & Zambolin, 2013) or for the cooling of photovoltaic modules in order to improve efficiency (Brötje, Kirchner, & Giovannetti, 2018). Studies concerning roll-bonded absorbers that form a sandwich panel are not yet available in the state of the science.

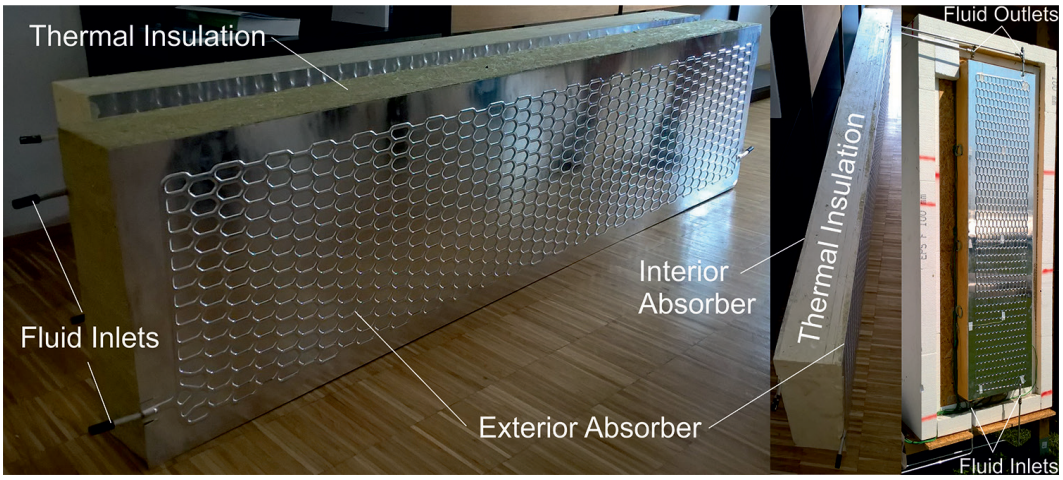

FIG. 1 Photos of a STAF panel equipped with blank aluminium absorbers and a honeycomb pipework

1.3 THERMAL AND STRUCTURAL ANALYSIS METHOD

The first of the two main objectives of this study is the analysis of the thermal behaviour of exterior absorber plates with the CFD (Computational Fluid Dynamics) method in order to optimise the fluid pipe design with regard to solar energy conversion. The second objective is to find an adequate structural analysis method to evaluate different installation situations of a STAF panel, considering the detailed thermal behaviour as boundary condition. In a first approach (Schober & Brandl, 2016) the thermal behaviour was determined with the help of the Software Fluent (ANSYS 18.2 release); the results were extracted at certain points of the exterior and interior absorber plates and used as boundary conditions in a FEM (Finite Element Method) model using the software Abaqus FEA (SIMULIA 6.14 release). Because these results were not accurate enough, another method is used in this study whereby the thermal behaviour and the resulting deformations are simulated with a so-called 'one-way coupled' simulation model (Feenstra, Hofmeyer, Van Herpen, & Mahendran, 2018). Literature shows some interesting findings concerning both numerical methods. For the paper of Ahmed, Leithner, Kosyna, and Wulff (2009), a coupled fluid dynamics and structural analysis for a boiler feed water pump was performed by the authors in order to predict its hydraulic and thermo-mechanical behaviour. In the study of Feenstra et al. (2018), two coupling approaches between CFD and FEM were used to perform CFD fire simulations as well as structural simulations of a room in a building. A one-way coupled CFD-FEM was also used for the analysis of the behaviour of a steel structure under natural fire by Malendowski and Glema (2017). There are a few more studies in which a coupled CFD-FEM simulation method was used (Fritsch et al. 2017; Zhang & Lu 2017; Liang, Luo, & Li, 2018; Kim, Choi, Park, Choi, & Lee, 2012; Peksen, 2015), but none dealt with the thermal and structural behaviour of sandwich panels. For the coupled simulation of this study, the software

platform ANSYS Workbench (ANSYS 18.2 release) is used, which includes CAD and meshing software as well as CFD and FEM simulation tools. The flow chart in Fig. 2 shows the setup of the one-way coupled CFD-FEM simulation.

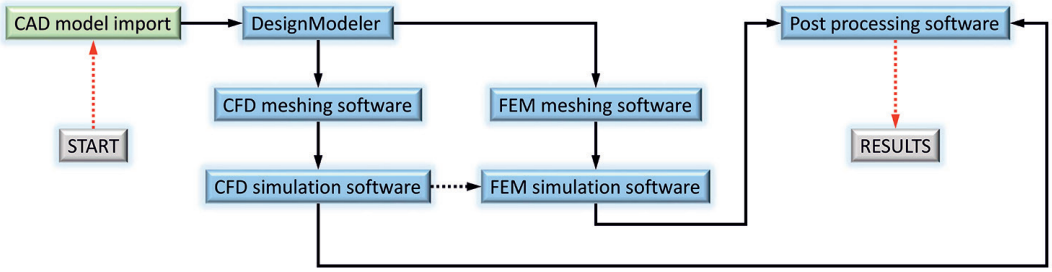

FIG. 2 Flow chart with the simulation setup of the one-way coupled CFD-FEM simulation

Usually, the CFD mesh must be much finer than the FEM mesh in order to consider the complex fluid characteristics, especially for the regions near walls. With the help of the CFD software Fluent, the flow characteristics and temperature distribution of the involved solid and fluid components is calculated. Furthermore, results from the CFD simulation can be used to determine the thermal output and the efficiency of the STAF panel´s exterior absorber. Afterwards, the resulting temperature characteristic of each solid from the CFD simulation serves as thermal boundary condition in the structural simulation (FEM model). With the FEM software from ANSYS, a structural analysis is performed under the influence of thermal deformations as well as deformations that are caused by external wind loads. The results from both simulations are transferred to the ANSYS Post Processing software where all results are evaluated and diagrams, contour plots etc. are created.

2 MEASUREMENTS IN AN OUTDOOR TEST FACILITY

2.1 DESCRIPTION OF THE MEASUREMENT SETUP

Over the course of the research project UNAB, an outdoor test facility was designed and assembled (Hörtenhuber, 2017) in order to use the monitored temperature data for the evaluation of the CFD model (Fig. 3). Furthermore, in the measurements, the comparison between a thermally activated and a non-activated STAF panel (= reference panel) can be observed. The reference panel is representative of a conventional sandwich panel forming the façade of an industrial building; for example, the STAF panel (shown in Fig. 1) consists of two equal absorber plates with the dimensions of 1.75 x 0.5m. The absorber with double-sided inflated fluid pipes has two aluminium plates with a thickness of 0.75mm per plate and the fluid pipes have a hydraulic diameter of 4.5mm. Additionally, the exterior absorber has a solar paint with an absorptivity of 0.95 and an emissivity of 0.85. Fig. 3 shows a photo of the test facility with the two façade elements that were installed in front of two thermally insulated boxes. Furthermore, this figure shows a photo from a thermographic camera, which was taken on 21st of September at 12:15. At this particular time, an actual global (horizontal) radiation of 707 W/m^2 was monitored while the exterior temperature was 16.6 °C. in addition, a very

low wind of approximately 0.35 m/s was measured. The exterior absorber of the STAF panel was supplied with water at a volume flow rate of 25.8 l/h and a temperature of 17.8 °C.

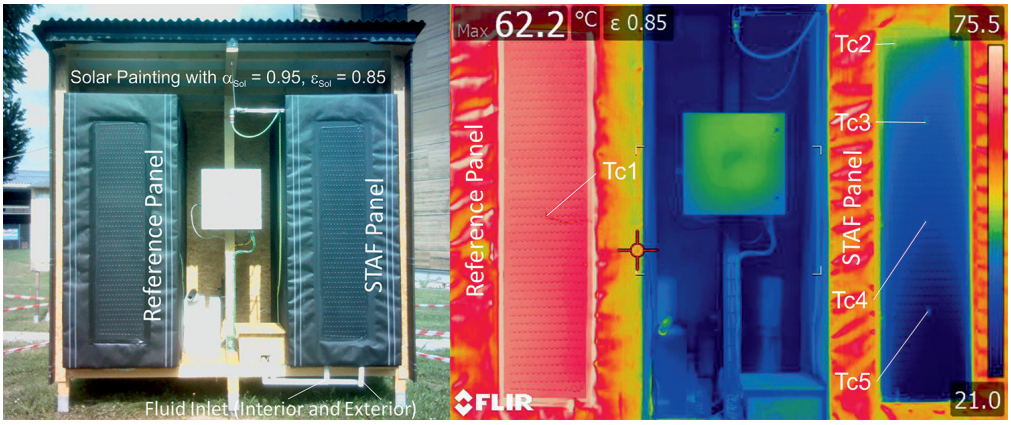

FIG. 3 (Left) Photo of the outdoor test facility. (Right) Thermographic photo during outdoor measurement (from 21st September 2016, 12:15). *(Image by M. Hörtenhuber, 2017).*

The water mass flow rate is monitored with the help of a magnetic-inductive flowmeter which has a measuring uncertainty of 2.5% of the measured value, but which is at least 0.05 l/h. The water temperature is monitored before the exterior absorber inlet as well as after the outlet with Pt100 sensors which have class A accuracy according to DIN EN 60751. The absorbers are equipped with a number of thermocouples (with class 1 accuracy) in order to measure the temperature at the exterior and the absorber plate´s surfaces, as well as inside the thermal insulation.

2.2 MEASUREMENT RESULTS

From 15th September, collected measurement data (shown in Fig. 4) serve as an example to give a short overview about the thermal behaviour of the STAF panel. The climate data are illustrated in the diagram on the left in Fig. 4. This diagram also includes the mass flow rate as well as the water inlet and outlet temperature of the exterior absorber of the STAF panel. The diagram on the right in Fig. 4 shows a comparison between the exterior absorber surface temperature of the reference and the STAF panel. Because the reference panel has an almost uniform temperature distribution, only one thermocouple (Tc1) is installed (illustrated in Fig. 3). The exterior absorber of the STAF panel shows an increasing surface temperature from the bottom to the top, which matches fluid motion that stores heat recovered from the absorption of solar radiation along the path (indicated by the temperature profiles of the thermocouples Tc2-Tc5). The difference between the hottest temperature of the STAF panel and the reference panel was approximately 25K. Furthermore, the maximum difference between water inlet and outlet temperatures occurred between 13:00 and 14:00 with an value of 21.3K, while the average mass flow was approximately 20kg/h over the day. In total, the energy harvesting for the panel on that day was approximately 3.48 kW/(m^2·d). Data were collected from the end of August until the end of November.

2.3 EFFICIENCY OF THE STAF PANEL´S EXTERIOR ABSORBER

With the help of all monitored data, the efficiency of the STAF panel´s exterior absorber is calculated according to the equation of the absorber efficiency (Duffie & Beckman, 1991; Streicher, 2007), which is illustrated in Fig. 5. The red line shows the linear regression of the set points which are calculated with the help of measurement data. The first term of this equation represents the conversion rate of the solar radiation. The second term of the equation considers the effect of convective heat loss of solar thermal collectors, whereas the third term represents the radiative heat loss. On the one hand, for the absorber of the STAF panel, the solar conversion is higher because of the missing glass cover that conventional solar thermal collectors have (shown as blue and green dashed lines in the diagram in Fig. 5).

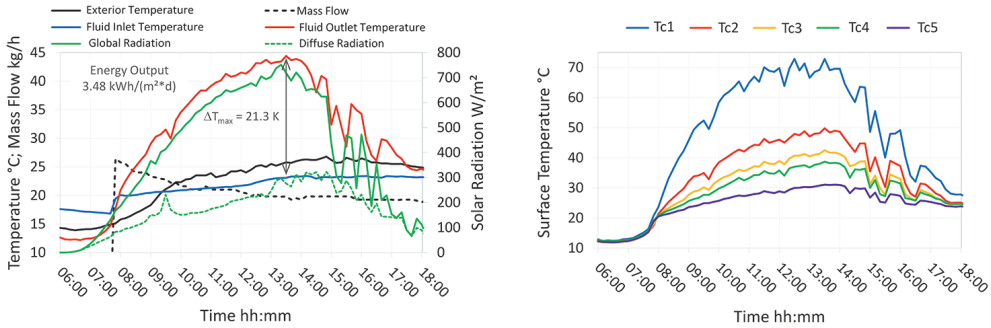

FIG. 4 Excerpt of measurement data from the outdoor test facility from 15th September 2016 between 06:00 and 18:00

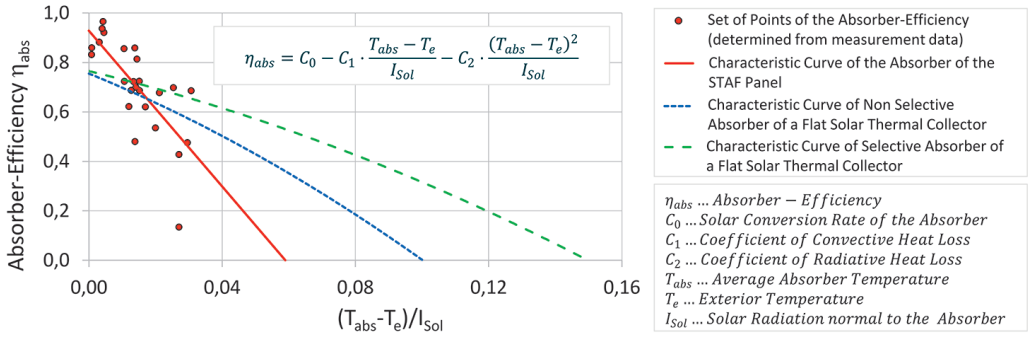

FIG. 5 Comparison of the efficiency between the STAF panel´s exterior absorber and solar thermal collectors

On the other hand, the convective heat loss is much higher when the exterior temperature is lower than the average absorber temperature. Compared to the convective heat loss, the radiative loss is so low that it can be neglected for the STAF panel´s exterior absorber. Generally, the efficiency of the STAF panel´s absorber can be described as good, but it cannot keep up with conventional solar thermal collectors without any improvements. The characteristic absorber efficiency curve can be used in a building and plant simulation in which the yearly energy output can be estimated by use of measured or generated climate data. Due to the scattering of the absorber efficiency's set points the RMSE (Root Mean Square Error) is 0.124, which is quite high. This scattering occurred because the uncovered absorber is strongly influenced by the wind, the conditions of which varied during the

outdoor measurements. For this reason, the characteristic curve must be divided into several curves that are created with the help of monitored values for the same wind.

3 THERMAL AND STRUCTURAL ANALYSIS OF THE STAF PANEL WITH COUPLED CFD-FEM SIMULATION METHOD

3.1 DESCRIPTION OF THE CFD MODEL

In order to optimise the absorber geometry, and to improve the fluid pipework, the Computational Fluid Dynamic simulation method was used. With this method, a various number of different absorber geometries (or only sections of an absorber) can be analysed at same exterior boundary conditions. For the proper design of the three-dimensional CFD model and to guarantee a good quality of the simulation results, the monitored data from a tested STAF panel were used. The absorber geometry is designed with the CAD tool, AutoCAD, and is later imported to the ANSYS DesignModeler in form of a Step-File. The CFD mesh and the definition and interconnection of all involved solid and fluid components, as well as the definition of boundary surfaces, are created with the Software ANSYS ICEM. Finally, in the CFD analysis, the simulation is performed in ANSYS Fluent after definition of the physical models and boundary conditions. In Fluent, the simulation is performed under steady state conditions using a 'Pressure-Based' solver. A section of the CFD mesh of the honeycomb absorber from measurement is shown in Fig. 6, together with the resulting water flow characteristic at the outlet region of the absorber's pipework.

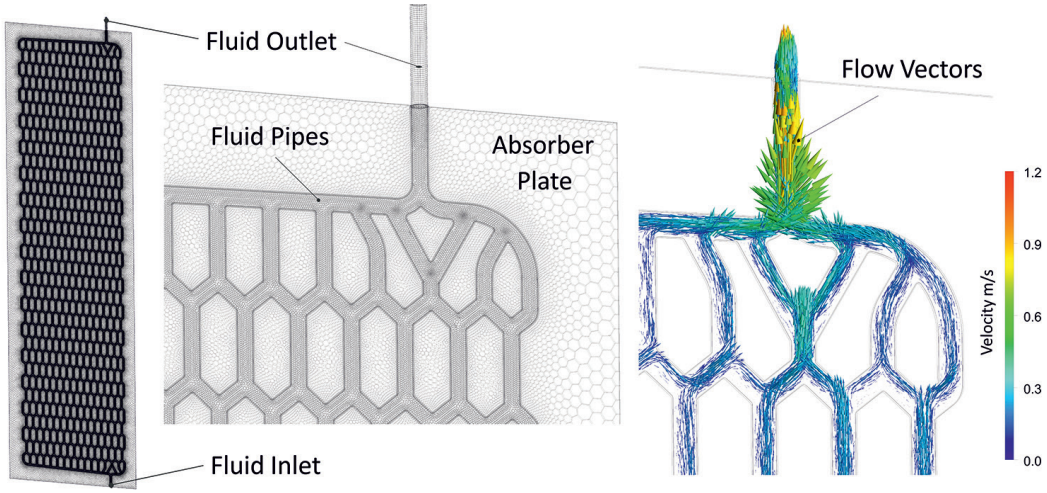

FIG. 6 Picture of the CFD mesh of the honeycomb absorber and a magnified section, with additional visualization of the fluid flow vectors

The final version of the mesh consists of approximately 25 million cells, after the tetrahedron cells are converted into polyhedral cells. This high number of cells is required because of the thin plates and the very flat shape of the fluid pipe. In particular, the fluid domain needs a special design in order to meet the requirements of the used 'Realizable k-e' turbulence model with an enhanced wall treatment. Both literature (Launder & Spalding, 1974) and the ANSYS User Guide state that this model is well suited for fluid dynamic simulations and combined heat transfer effects. Several CFD

analyses, regarding thermal behaviour, heat transfer effects, and effects of natural convection, were performed by two of the involved authors (Brandl, Mach, Grobbauer, Hochenauer, 2014; Brandl et al. 2015; Brandl, Mach, & Hochenauer, 2016) in the past. Nevertheless, in this study, different CFD model approaches are also compared and evaluated with the help of the measurement results (see Section 3.2). Furthermore, the fluid inlet is defined as mass flow inlet with the mass flow rate and the fluid inlet temperature as boundary conditions, whereas the fluid outlet is defined as a pressure outlet in the simulation model. At the exterior wall, an outdoor temperature and a solar radiation are defined as boundary conditions, as well as a convective heat transfer coefficient representing the influence of natural convection and wind.

The solar radiation is considered in the form of a radiation temperature (T_{rad} in K) according to the following equation (1) which is derived from Stefan-Boltzmann law. I is the radiation in W/m^2, T_e is the exterior temperature in K, and s is the Stefan-Boltzmann constant (= 5.67e-8 W/(m^{2}K^4)).

$$T_{rad} = \left(T_e^4 + \frac{I}{\sigma} \right)^{0.25}$$

At the inner wall, an interior room temperature and a heat transfer coefficient are defined.
The thermal insulation and the interior plate are considered as virtual layers in the CFD model of the STAF panel with the honeycomb absorber, while real solid and fluid bodies are created in the example of the CFD-FEM coupling (presented in Chapter 3.4). The external heat transfer coefficient a_e in W/(m^{2}K) is calculated according to the following equation (2) from standard VDI 2055. In this equation, L stands for the façade´s height in m and v for the wind speed in m/s.

$$\alpha_e = 3.96 \cdot (v/L)^{0.5}; for (v/L) < 8m^2/s$$
$$\alpha_e = 11/L + 5.8 \cdot [(L \cdot v - 8)/(L \cdot v)] \cdot (v^4/L)^{0.2}; for (v/L) > 8m^2/s$$

3.2 COMPARISON OF THE THERMAL BEHAVIOUR BETWEEN MEASUREMENT AND CFD SIMULATION

Before performing the thermal analysis of the absorber with different fluid pipe designs, the CFD model is evaluated by comparing the temperature data of the STAF panel with the honeycomb absorber, which was installed in an outdoor test facility. In the comparison, the evaluated thermographic photos and the measured water outlet temperature are used. Furthermore, measured values are used as boundary conditions in the CFD model. For this purpose, the data from 21st September are most suitable. At 12:09, a global radiation of 737 W/m^2 perpendicular to the STAF panel was measured with a diffuse fraction of 244 W/m^2. An exterior temperature of 16.6 °C was measured, and the averaged value of the wind speed between 12:00 and 13:00 resulted in a value of 0.35 m/s (= very low wind). The thermocouples inside the box behind the STAF panel measured an average interior temperature of 15.4 °C at that time. The mass flow rate was 25.5 kg/h and the

supplied water had a temperature of 17.8 °C. In the CFD model, the water has a density of 998.2 kg/m^3, a specific heat of 4182 J/kgK, and a thermal conductivity of 0.4 W/mK. The absorbers are made of aluminium with a density of 2700 kg/m^3, a specific heat capacity of 896 J/kgK, and a high thermal conductivity of 201 W/mK. Polyurethane is used as thermal insulation between the exterior and interior absorber plate, which has a density of 80 kg/m^3, a specific heat capacity of 1400 J/kgK, and a thermal conductivity of 0.025 W/mK. Because the water supply pipe is partly exposed to the sun, a preliminary CFD simulation, only of this pipe, was performed for the following comparison between measurement and CFD simulations (Fig. 7). The same model parameters are used in the CFD model as in the simulation of the STAF panel. A temperature difference of 0.48K between the measurement sensor and the mass flow inlet of the CFD model of the STAF panel is the result of this preliminary simulation. Therefore, in the CFD model of the STAF panel, a water inlet temperature of 18.3 °C is defined as the boundary condition. In the comparison between the measurement and CFD simulation, a couple of different models were used in order to choose the most suitable model for further analysis. The initial CFD model, which is described in the text above, uses a constant density for the fluid. In the next CFD model the 'Gravity' is activated as well as the option 'Full Buoyancy Effects' in the turbulence model. Furthermore, the density of the fluid is defined as piecewise linear depending on the fluid temperature to enable natural convection inside the pipes of the absorber plate.

A last version of the STAF CFD model is an extension of the model with natural convection. An air-filled domain of 1m is added in front of the exterior absorber which has an inlet and outlet surface (Fig. 7). In this model, the boundary condition of the exterior temperature and the heat transfer coefficient, as well as the external radiation temperature are removed. Instead of the external radiation temperature, the solar calculator from FLUENT is used.

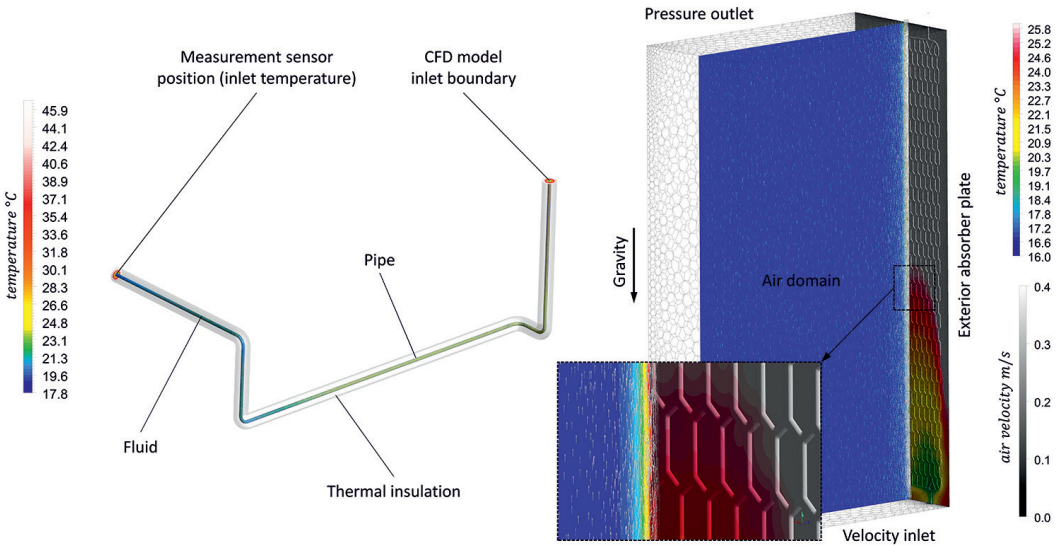

FIG. 7 Temperature contours of the water supply pipe CFD model (left), STAF CFD model with additional air domain (right)

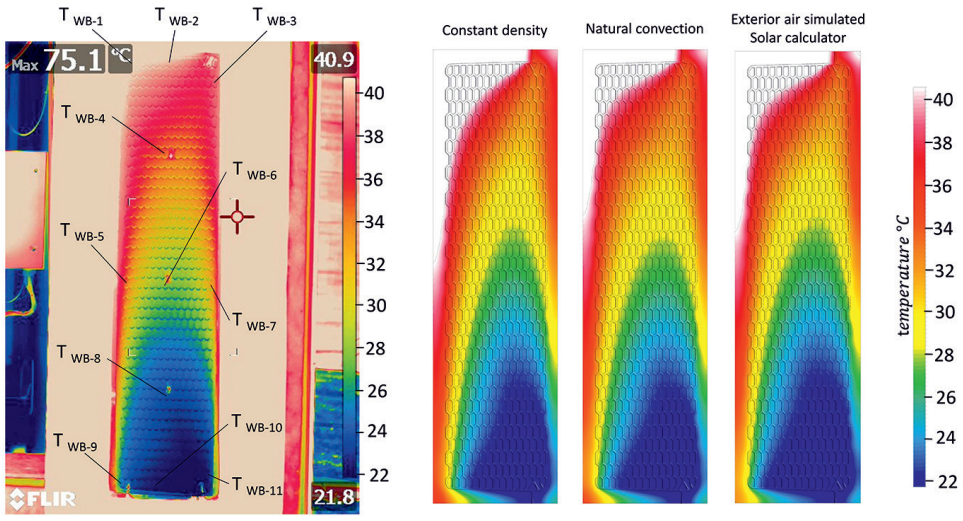

FIG. 8 Comparison between temperature contours from CDF simulations and the thermographic photo (from 21st September 2016, 12:09) of the STAF panel´s exterior absorber

POSITION	Thermo-graphic analysis (TA)	CFD Constant density (CD)	Difference between TA and CD	CFD Natural convection (NC)	Difference between TA and NC	CFD Exterior air and Solar calculator (EASC)	Difference between TA and EASC
	°C	°C	K	°C	K	°C	K
T_{WB-1}	48.1	51.8	3.7	47.7	0.4	46.2	1.9
T_{WB-2}	42.0	44.8	2.8	42.7	0.7	43.4	1.4
T_{WB-3}	36.4	34.5	1.9	34.9	1.5	34.9	1.5
T_{WB-4}	33.2	31.8	1.4	31.7	1.5	31.1	2.1
T_{WB-5}	33.7	36.0	2.3	34.4	0.7	34.1	0.4
T_{WB-6}	29.1	29.5	0.4	29.5	0.4	28.9	0.2
T_{WB-7}	31.5	30.2	1.3	30.4	1.1	29.7	1.8
T_{WB-8}	25.7	24.7	1.0	24.6	1.1	23.9	1.8
T_{WB-9}	27.4	28.6	1.2	27.0	0.4	25.8	1.6
T_{WB-10}	23.1	21.4	1.7	21.4	1.7	20.8	2.3
T_{WB-11}	23.8	20.9	2.9	20.9	2.9	20.9	2.9

TABLE 1 Comparison of surface temperatures of the exterior absorber plate between thermographic analysis (from 21st September 2016, 12:09) and the CFD simulation results

Fig. 8 shows the comparison between a thermographic photo and the resulting temperature contours of the exterior absorber from CFD simulations. Additionally, those positions are indicated where the temperature of the thermographic photo is evaluated (with the help of the software 'ResearchIR') and compared to the simulation results. A summary of this comparison can be found in Table 1. Generally, all temperature characteristics look similar. Considering the comparison of the water outlet temperature that is measured and simulated, data match very well. The difference between the investigated measured and simulated values at exterior temperatures of the absorber plate is a deviation between 3.7 and 2.9K. Because the CFD model with natural convection shows a better agreement with the thermographic photo and the evaluated temperatures, this model is proposed for further analyses with varying fluid pipe designs. A comparison between simulated and measured water outlet temperatures and the resulting thermal output from other days is

also performed. The results are summarised in Table 2 and show a good agreement between measurement and simulation.

DATE	TIME	EXTERIOR TEMP.	SOLAR RADIATION	MASS FLOW RATE	FLUID INLET TEMP.	DT-PIPE-SUPPLY (SIM.)	FLUID OUTLET TEMP. (MEAS.)	FLUID OUTLET TEMP. (SIM.)	THERMAL OUTPUT (MEAS.)	THERMAL OUTPUT (SIM.)
dd.mm.yyyy	hh:mm	°C	W/m^2	kg/s	°C	°C	°C	°C	W/m^2	W/m^2
01.09.2016	12:00	25.6	630	0.0124	25.7	0.22	28.8	28.4	185	162
02.09.2016	12:00	27.1	652	0.0075	24.7	0.38	30.2	29.5	197	174
20.09.2016	14:02	17.5	621	0.0031	20.1	0.55	48.9	49.1	432	435
21.09.2016	12:09	16.6	737	0.0071	17.8	0.48	36.9	36.3	644	627
23.09.2016	13:00	20.4	749	0.0063	18.2	0.41	38.6	38.5	617	614

TABLE 2 Comparison of water outlet temperature and the thermal output between measurement and CFD simulation at different times

3.3 RESULTS FROM THERMAL ANALYSIS (CFD)

After the positive evaluation of the numerical method and the CFD model, this study shows the analysis of the thermal behaviour and thermal output of three further pipe designs for the absorber plate, with the dimensions 1.75 x 0.5m. For this analysis, the following boundary conditions are used: a solar radiation of 1000 W/m^2 at an angle of 45 °; an exterior temperature of 30 °C and a heat transfer coefficient of 25 W/m^2K; an interior temperature of 20 °C and a heat transfer coefficient of 5 W/m^2K; a fluid inlet temperature of 15 °C and a mass flow rate of 50 kg/h; and a solar absorptivity of 0.95 for the exterior absorber surface. The comparison includes four different layouts: (a) the honeycomb absorber which is also used in the comparison with the in-situ measurements, (b) a harp absorber with 14 vertical, parallel fluid pipes, (c) again a harp absorber but with only 10 fluid pipes, and (d) another harp absorber but with 11 vertical, parallel arranged fluid pipes and more complex inlet and outlet pipework. The computed temperature contours of these four absorbers are illustrated in Fig. 9. All absorbers have (f) one-sided inflated fluid pipes, except the honeycomb absorber which has (e) double-sided inflated pipes. The relevant results from CFD simulations are summarised in Table 3.

The highest water outlet temperature of 27.9 °C is achieved with the absorber with 14 vertical fluid pipes (b) followed by the honeycomb absorber for which the fluid outlet temperature is 27.8 °C, and the absorber with 10 pipes which has a water outlet temperature of 27.7 °C. The lowest fluid outlet temperature (27.4 °C) occurs for the absorber (d) with the more complex inlet and outlet geometry. The resulting thermal output is 857 W/m^2 for the absorber (b), 851 W/m^2 for absorber (a), 846 W/m^2 for absorber (c), and 822 W/m^2 for absorber (d). The honeycomb absorber (a) with the double-sided inflated fluid pipe shows the lowest pressure difference of 1056 Pa between water inlet and outlet. The absorber (b) with the 14 pipes shows a pressure difference of 1424 Pa and 1599 Pa for the absorber (c) with 10 pipes. Again, the absorber (d) shows the worst case with a pressure difference of 2936 Pa.

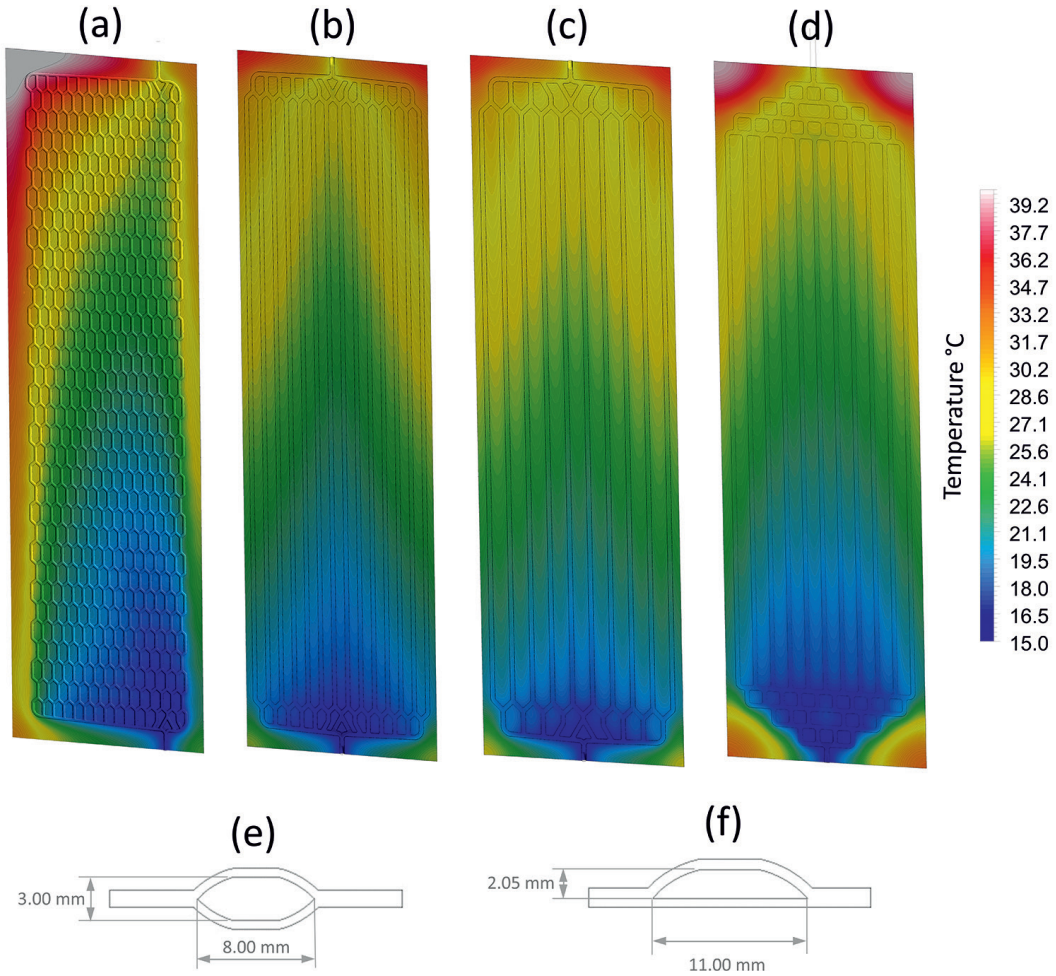

FIG. 9 Illustration of the absorber temperature contours of an absorber with a (a) honeycomb, (b) 14 vertical pipe harp, (c) 10 vertical pipe harp, and (d) 11 vertical pipe harp absorber. Schematic (e) shows the cross section of the double-sided inflated pipe profile, and (f) of the one-sided inflated pipe profile.

PIPE DESIGN	FLUID OUTLET TEMPERATURE	THERMAL OUTPUT	PRESSURE DIFFERENCE
	°C	W/m²	Pa
Honeycomb	27.8	851	1056
Harp, 14 vertical pipes	27.9	857	1424
Harp, 10 vertical pipes	27.7	846	1599
Harp, 11 vertical pipes	27.4	822	2936

TABLE 3 Comparison of the water outlet temperature, the thermal output, and the pressure difference between the absorber designs

3.4 DESCRIPTION AND RESULTS FROM STRUCTURAL ANALYSIS (FEM)

The thermal analysis is followed by a structural analysis in which the deformation of the STAF panel is simulated with the help of the Finite Element Method (FEM). The same CFD model is used as a basis for the model, but the mesh is much coarser. Furthermore, the fluid domain is not necessary in the FEM simulation and can be neglected in the model. In the structural analysis, the thermal

deformations are considered, as well as the pressure caused by wind loads. Two different wind characteristics are observed: low wind and strong wind. While, for low wind the pressure is very small, a dynamic pressure p_d of 1000 Pa is set as an additional boundary condition in the FEM model with strong wind. The dynamic pressure of 1000 Pa represents a wind speed of approximately 150 km/h according to equation (3), which is more than the maximum occurring wind in the region of Austria. The external heat transfer coefficient is increasing to a value of 100 W/m^{2}K according to equation (2). In the equation r is the density of the fluid in kg/m^3 and v is the wind speed in m/s.

$$p_d = \frac{1}{2} \cdot \rho \cdot v^2$$

For the determination of the thermal deformations, the results from the thermal analysis (CFD) are used as boundary conditions. For this reason, the temperature characteristic of each solid body is imported in the FEM model. This study presents the comparison of the deformation between a 3.5 x 1.0 x 0.15m STAF panel and a conventional aluminium sandwich panel with polyurethane foam as the thermal insulator, and which has the same dimensions as the STAF panel. One-sided inflated fluid pipes are used, and the absorber plates show a thickness of 1.5mm. The STAF panel contains 20 vertical fluid pipes which have individual inlets and outlets. The water is evenly supplied to the pipes (exterior and interior sides) at the bottom of the STAF panel with a mass flow rate of 100 kg/h and the water inlet temperature is measured at 10°C. At the exterior side, the water is heated due to 1000 W/m^2 solar radiation and a solar angle of 45°, while the exterior temperature is 30°C. At the interior side of the panel, a room temperature of 25°C is defined. The heat transfer coefficients and absorptivity have the same values as in the simulation in Chapter 3.3. Fig. 10 shows the resulting temperature profiles from CFD simulation (a-d) as well as the deformations from FEM simulation (e-h) of the conventional sandwich and the STAF panel. The maximum deformations occurred at the middle of the panel for the conventional sandwich panel and slightly above the middle for the STAF panel. Under low wind conditions, the maximum deformation is approximately 6.5mm for the conventional panel and about 3.6mm for this version of the STAF panel. Under strong wind, the maximum deformation is generally higher, with values of 17.5mm for the conventional sandwich panel and 15.6mm for the STAF panel. The results from CFD and FEM simulations are summarised in Table 4.

	AVERAGED SURFACE TEMPERATURE FOR LOW WIND	AVERAGED SURFACE TEMPERATURE FOR STRONG WIND	MAXIMUM DEFORMATION FOR LOW WIND	MAXIMUM DEFORMATION FOR STRONG WIND
	°C	°C	mm	mm
Exterior plate STAF panel	25.3	28.6	3.6	15.6
Interior plate STAF panel	12.2	12.2	3.6	15.6
Exterior plate sandwich panel	51.1	36.3	6.5	17.5
Interior plate sandwich panel	25.8	25.4	6.5	17.5

TABLE 4 Summary of the averaged surface temperature of the exterior and the interior absorber and the simulated maximum deformations

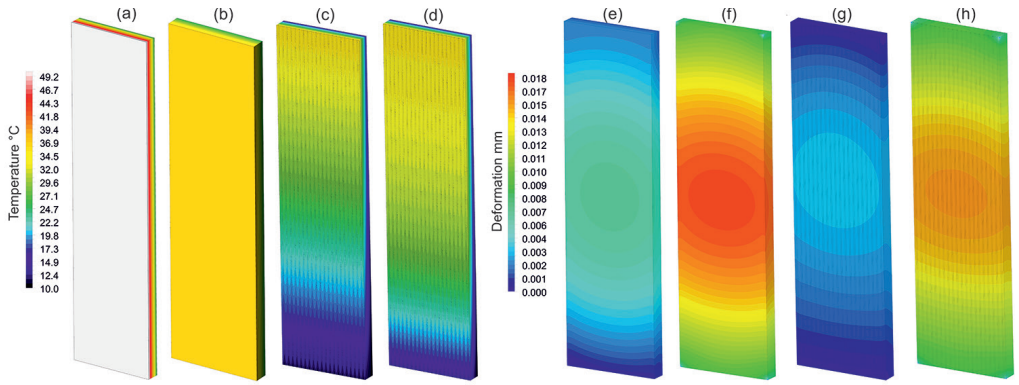

FIG. 10 Temperature contours of (a) the sandwich panel for low wind, (b) sandwich panel for strong wind, (c) STAF panel for low wind, (d) STAF panel for strong wind. Deformation of the (e) sandwich panel for low wind, (f) sandwich panel for strong wind, (g) STAF panel for low wind, (h) STAF panel for strong wind.

4 CONCLUSION AND OUTLOOK

In order to fulfil one of the main objectives of this study (mentioned in Section 1.3), the 'one-way coupling' between the two numerical simulation methods CFD-FEM has been implemented and allows the determination of the deformations caused by heat and cooling effects and/or wind loads.

Furthermore, the CFD model was evaluated with the help of measurement data from an outdoor test facility and thermographic photos of the STAF panel´s exterior absorber. A good agreement was achieved between the measured and simulated water outlet temperature of an absorber with a honeycomb pipework. Furthermore, from the comparison of the temperature noted between the CFD simulation and the thermographic images, it was concluded that the CFD model is accurate enough for further analyses.

In order to optimise the pipe design of the STAF panel with a honeycomb absorber from the outdoor test facility (and fulfil the remaining main objective of this study), three further absorber geometries were designed and analysed with the help of CFD simulations. The absorber with the 14 vertical, parallel arranged fluid pipes with one side inflation shows the best thermal performance. The lowest pressure difference was achieved for the honeycomb absorber with double-sided inflated fluid pipes.

From the results of the FEM simulation, it was concluded that the static behaviour was slightly improved due to the integrated fluid pipes. Generally, the mechanical stresses and thermal deformations are within the acceptable tolerances.

Based on the completed and pending thermal and static analyses, prototypes will be produced and measured under real climate conditions. The measurement data can be used for a final optimisation of the STAF panel. Therefore, a new outdoor test facility will be installed, which will allow the parallel analysis of five STAF panels.

Acknowledgements

All contents of this publication are part of the already completed project 'Umsetzung nachhaltigen Bauens durch optimierte Projektsteuerungsprozesse und integrale Gebäudehüllen' (UNAB), which was funded by the 'Zukunftsfonds Steiermark' des Landes Steiermark, as well as of the ongoing Interreg-project 'ABS-Network SIAT 125' at Graz University of Technology, Austria. Interreg V-A Slovenia-Austria is a cross-border cooperation programme between Slovenia and Austria in the programme period 2014-2020. An overview of the project and a list of all participants can be found at the following link: http://abs-network.eu/en

References

Ahmed, S., Leithner, R., Kosyna, G., & Wulff, D. (2009). Increasing reliability using FEM–CFD. *World Pumps, 509*, pp.35-39.

BKI Baukosteninformationszentrum [Construction Costs Information Center] (2018). BKI Baukosten Neubau 2018 - Teil 1-3 [Construction costs of new buildings 2018 - part 1-3] : Statistische Kostenkennwerte Gebäude, Positionen und Bauelemente [Statistical cost factors of buildings, positions and parts]. Stuttgart: BKI 2018.

Brandl, D., Mach, T., Grobbauer, M., Hochenauer, C. (2014). Analysis of ventilation effects and the thermal behaviour of multifunctional façade elements with 3D CFD models. *Energy and Buildings, 85*, pp.305-320.

Brandl, D., Mach, T., Kaltenecker, P., Sterrer, R., Neururer, C., Treberspurg, M., & Hochenauer, C. (2015). CFD assessment of a solar honeycomb (SHC) façade element with integrated PV cells. *Solar Energy, 118*, pp.155-174.

Brandl, D., Mach, T., & Hochenauer, C. (2016). Analysis of the transient thermal behaviour of a solar honeycomb (SHC) façade element with and without integrated PV cells. *Solar Energy, 123*, pp.1-16.

Brötje, S., Kirchner, M., & Giovannetti, F. (2018). Performance and heat transfer analysis of uncovered photovoltaic-thermal collectors with detachable compound. *Solar Energy, 170*, pp.406-418.

Brucha Ges.m.b.H. (1948). Retrieved from http://www.brucha.com/

Del Col, D., Padovan, A., Bortolato, M., Dai Prè, M., & Zambolin, E. (2013). Thermal performance of flat plate solar collectors with sheet-and-tube and roll-bond absorbers. *Energy, 58*, pp.258-269.

Duffie, J. & Beckman, W. (1991). *Solar engineering of thermal processes.* New York: Wiley-Interscience Publication, John Wiley & Sons, Inc.

Ebrahimi, H., Someh, L. K., Norato, J., & Vaziri, A. (2018). Blast-resilience of honeycomb sandwich panels. *International Journal of Mechanical Sciences, 144*, pp.1-9.

Eizadjou, M., Manesh, H. D., & Janghorban, K. (2009). Mechanism of warm and cold roll bonding of aluminum alloy strips. *Materials & Design, 30,* 10, pp.4156-4161.

EN 14509 (2013). *Self-supporting double skin metal faced insulating panels – Factory made products – Specifications*.

Feenstra, J.A., Hofmeyer, H., Van Herpen, R.A.P., & Mahendran, M. (2018). Automated two-way coupling of CFD fire simulations to thermomechanical FE analyses at the overall structural level, *Fire Safety Journal, 96*, pp.165-175.

Fritsch, A., Uhlig, R., Marocco, L., Frantz, C., Flesch, R., & Hoffschmidt, B. (2017). A comparison between transient CFD and FEM simulations of solar central receiver tubes using molten salt and liquid metals, *Solar Energy, 155*, 2017, pp.259-266.

Haseli, M., Layeghi, M., & Hosseinabadi, H. Z. (2018). Characterization of blockboard and battenboard sandwich panels from date palm waste trunks. *Measurement, 124*, pp.329-337.

Hashemi, S. J., Razzaghi, J., Moghadam, A. S., & Lourenço, P. B. (2018). Cyclic testing of steel frames infilled with concrete sandwich panels. *Archives of Civil and Mechanical Engineering, 18*, 2, pp.557-572.

Hermes, C.J.L., Melo, C., & Negrão, C.O.R. (2008). A numerical simulation model for plate-type, roll-bond evaporators. *International Journal of Refrigeration, 31*, 2, pp.335-347.

Hörtenhuber, M. (2017). *Konstruktion, Aufbau und Inbetriebnahme eines Versuchsstandes zur Ermittlung des thermischen Verhaltens eines integralen Fassadenelementes* [Construction, assembly and commissioning of an experimental test stand for the analysis of the thermal behaviour of an integral façade element]. Graz: Technische Universität Graz

IC Market Tracking (2016). *Sandwichpaneele in Europa* [Sandwich panels in europe]. Retrieved from https://www.interconnection-consulting.com/de/industry/119

Kim, S., Choi, J., Park, J., Choi, Y., & Lee, J. (2013). A coupled CFD-FEM analysis on the safety injection subjected to thermal stratification. *Nuclear Engineering and Technology, 45, 2*, pp.237-248.

Koschade, R. (2011). *Sandwichbauweise: Konstruktion, Systembauteile, Ökologie (Detail Spezial) [Sandwich construction: construction, system components, ecology (detail special)]*, Inst. f. Int. Architektur Dokumentation [Institute of int. architecture documentation].

Launder, B.E. & Spalding, D.B. (1974). The numerical computation of turbulent flows. *Computer Methods in Applied Mechanics and Engineering, 3, 2*, pp.269-289.

Li, Z. Zheng, Z., Yu, J., & Lu, F. (2017). Deformation and perforation of sandwich panels with aluminum-foam core at elevated temperatures, *International Journal of Impact Engineering, 109*, pp.366-377.

Liang, R., Luo, Y., & Li, Z. (2018). The effect of humping on residual stress and distortion in high-speed laser welding using coupled CFD-FEM model, *Optics & Laser Technology*, 104, pp.201-205.

Malendowski, M., & Glema, A. (2017). Development and Implementation of Coupling Method for CFD-FEM Analyses of Steel Structures in Natural Fire, *Procedia Engineering, 172*, pp.692-700.

Missoum, S., Lacaze, S, Amabili, M., & Alijani, F., (2017). Identification of material properties of composite sandwich panels under geometric uncertainty. *Composite Structures, 179*, pp.695-704.

Peksen, M. (2015). 3D CFD/FEM analysis of thermomechanical long-term behaviour in SOFCs: Furnace operation with different fuel gases. *International Journal of Hydrogen Energy, 40*, 36, pp.12362-12369.

Quintana, J. M., & Mower, T. M. (2017). Thermomechanical behavior of sandwich panels with graphitic-foam cores. *Materials & Design, 135*, pp.411-422.

Ravi, P. S., Krishnaiah, A., Akella,S., & Azizuddin, M. (2015). Evaluation of Inside Heat Transfer Coefficient of Roll Bond Evaporator for Room Air Conditioner. *International Journal of Innovative Research in Science, Engineering and Technology, 4, 5*, pp.3378-3384.

Righetti, G., Zilio, C., & Longo, G. A. (2014). Experimental Analysis of R134a and R1234ze (E)Flow Boiling Inside a Roll Bond Evaporator, *International Refrigeration and Air Conditioning Conference, Paper 1404*.

Schober, H. & Brandl, D. (2016). Integrale Gebäudehüllen - Entwicklung eines solarthermisch aktivierten, multifunktionalen Fassadenpaneels [Integral building envelopes - Development of a solar thermally activated, multifunctional façade panel], *Gleisdorf SOLAR 2016 - Internationale Konferenz für solares Heizen und Kühlen, Gleisdorf, Österreich*.

Streicher, W. (2007). Sonnenergienutzung (Vorlesungsskriptum) [Use of solar energy (lecture script)], Institut für Wärmetechnik: Technische Universität Graz.

Sun, X., Wu, J., Dai, Y., & Wang, R. (2014). Experimental study on roll-bond collector/evaporator with optimized-channel used in direct expansion solar assisted heat pump water heating system, *Applied Thermal Engineering, 66*, 1–2, pp.571-579.

Talum d.d. (1942). Retrieved from http://www.talum.si/.

Yazdani Sarvestani, H. , Akbarzadeh, A.H., Niknam, H., & Hermenean, K. (2018). 3D printed architected polymeric sandwich panels: Energy absorption and structural performance, *Composite Structures, 200*, pp.886-909.

Yuan, W., Wang, J., Song, H., Ma, T., Wu, W., Li, J., & Huang, C. (2018). High-power laser resistance of filled sandwich panel with truss core: An experimental study. *Composite Structures, 193*, pp.53-62.

Zhang, Y., & Lu, T. (2017). Unsteady-state thermal stress and thermal deformation analysis for a pressurizer surge line subjected to thermal stratification based on a coupled CFD-FEM method. *Annals of Nuclear Energy, 108*, pp.253-267.